Chemical Stability and Characterization of Rhodium-Diisocyanide Coordination Polymers

Cantwell G. Carson,[†] Rosario A. Gerhardt,[†] and Rina Tannenbaum*[,†,‡]

School of Materials Science and Engineering, Georgia Institute of Technology, Atlanta, Georgia, and Department of Chemical Engineering, Technion—Israel Institute of Technology, Haifa, Israel

Received: August 15, 2007; In Final Form: October 1, 2007

Poly-[Rh(1,4-phenylene diisocyanide)$^{+}_{4/2}$(Cl)$^{-}$] has a two-dimensional template structure, where Rh atoms are bonded by the π-conjugated 1,4-phenylene diisocyanide (pdi) ligands in the $x-y$ plane and through overlapping d_z orbitals in the z direction. The more conductive metallic bonds in the z direction create anisotropy in the electrical conductivity. The anisotropy and unique geometry of poly-[Rh(pdi)$^{+}_{4/2}$(Cl)$^{-}$] make it a useful test bed for examining the relationship between electrical properties and chemical stability in metal−isocyanide molecular wire systems. The bulk powder of poly-[Rh(pdi)$^{+}_{4/2}$(Cl)$^{-}$] is estimated to have a room-temperature bulk conductivity of 3.4×10^{-11} S·cm^{-1}, an electrical activation energy of 0.9 eV, and a dielectric constant of 7.5. In this paper, impedance spectroscopy and X-ray powder diffraction were used to show the dependence of the electrical conductivity on the metal−metal bonding of pressed bulk powders of poly-[Rh(pdi)$^{+}_{4/2}$(Cl)$^{-}$]. Thermo-gravimetric analysis and X-ray photoelectron spectroscopy were used to demonstrate air sensitivity in the polymer and elucidate the mechanism of oxidative degradation.

1. Introduction

Molecular electronics has been an area of recent interest. This has been driven principally by the potential to utilize synthetic molecules and short-chain oligomers as wires,[1−4] rectifiers,[5,6] transistors,[7] and switches.[8] This research very often entails the use of a "bottom up" approach to the fabrication of microelectronic devices through the intermediacy of self-assembled monolayers (SAM).[1,4−6,9,10] The advantage of this approach is that molecules on smooth metal surfaces can assemble into specific and regular arrangements. The two-dimensional nature of this approach makes the comparison of the electrical properties of different molecules and substrates fairly straightforward. Moreover, the electrical properties of these potentially conductive molecules have also been examined after being coordinated to individual metal ions in solution. By studying these materials either in the bulk or in the solution phase, it becomes possible to also observe the effects of different architectures and crystal structures on their electrical properties.[11−15] This approach offers a way to explore the discrete behavior and stability of the conduction mechanisms of these organic molecules, which is not otherwise available with SAM methods.

One of the most promising platforms to probe discrete electrical properties of molecular species is in the context of coordination polymers. These are formed when potentially conducting organic molecules with electron-donor properties are coordinatively bonded to discrete metallic centers to form macromolecular structures. More specifically, coordination polymers represent a class of materials in which bi-dentate, nonchelating ligands act as coordination bridges between metal centers to form polymers having 1, 2, or 3 dimensions, depending on the coordination geometry of the metals.[14−25] The choice of metallic centers, ligands, and substituents allows for flexibility in tailoring the chemical, optical, physical, and electrical properties. As a result, these polymers have attracted attention due to their potential application in solid-state devices and catalytic processes.[14] The class of coordination polymers that contains metal atoms as an integral part of the main chain is of special interest, as this allows us to characterize the effect of structure and chemistry on the electrical properties of the metal−ligand bond.

Coordination polymers are generally insulating. However, conduction bands can be created with the proper choice of ligand, metal center, and the position of that metal center in the polymer chain.[16,17] For example, the resonance effect of π-conjugated molecules coordinated between metallic centers can generate an effective semiconducting mechanism. In addition, conduction bands can arise when large numbers of adjacent metal atoms are close enough to promote overlap of their d_z orbitals. In both scenarios, free electrons can then move from one metal atom to the next or along the π bonds in the π-conjugated molecular bridges. If there are enough of these atoms or molecules connected in such a fashion, then the conductivity of the material can be greatly increased by the presence of these extended conducting chains.[16,17]

These types of coordination polymers can optimally be synthesized by utilizing linear, bidentate, rigid ligands and metallic centers with square-planar coordination geometry. For the current study, 1,4-phenylene diisocyanide (pdi) was chosen because of its rigid, π-conjugated backbone and its ability to form strong, linear ligand-to-metal coordination bonds (acting as an effective π acid).[18−24] In addition, the electrical behavior of the metal−isocyanide bond has been a recent area of interest because of its low conduction barrier.[1] It has also been shown to displace CO in metal−carbonyl complexes, which are common precursors for other organometallic compounds.[25] Rh(I) was used as a d^6 metal center because it possesses square-planar coordination geometry and its carbonyl complex precursor is commercially available. The product, poly-[Rh(pdi)$^{+}_{4/2}$(Cl)$^{-}$], is an ideal test bed for studying the relation-

* Corresponding author. E-mail: rinatan@mse.gatech.edu.
[†] Georgia Institute of Technology.
[‡] Technion—Israel Institute of Technology.

10.1021/jp0765852 CCC: $37.00
Published on Web 11/30/2007

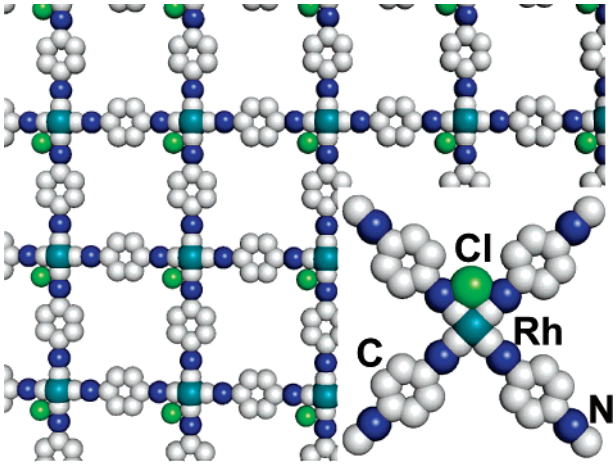

Figure 1. Schematic representation of poly-[Rh(pdi)$^{+}_{4/2}$(Cl)$^{-}$] square planar two-dimensional network. The inset shows a model of a monomer, with atoms labeled.

ship between structure, chemistry, and electrical properties in metal−isocyanide complexes. As the idealized model in Figure 1 shows, the reaction between $[Rh(CO)_2Cl]_2$ and pdi creates a sheet-like square grid of Rh(I) atoms separated by rigid pdi ligands. The π-conjugated pdi ligands allow for extended π conjugation throughout the whole polymer while the weak attraction between metal atoms on adjacent sheets causes polymer sheets to stack, aligning Rh(I) atoms into connected columnar chains.[17]

Although this is not the first report of the electrical properties of poly-[Rh(pdi)$^{+}_{4/2}$(Cl)$^{-}$],[16] new methods and instrumentation are now available to clarify the physical basis for the electrical semiconductivity of this class of materials and examine their chemical stability. The analysis of electrical properties under alternating current (AC), or impedance spectroscopy, reveals the collective response of microscopic polarization processes under an applied external AC electric field.[26] Under an AC field, frequency dispersion can be observed by measuring the impedance and susceptibility of a given material due to the different polarization and relaxation mechanisms present.[27] The complex impedance $Z^*(\omega)$ and the complex permittivity $\epsilon^*(\omega)$ are obtained as a function of frequency as follows:[28]

$$\epsilon^* = \epsilon' - j\epsilon'' \quad \text{and} \quad Z^* = Z' - jZ'' = \frac{1}{j\omega\epsilon^* C_0} \qquad (1)$$

where $j = \sqrt{-1}$ and ω is the frequency in radians. The real parts are denoted by a single prime (ϵ' and Z'), and the imaginary parts are denoted by a double prime (ϵ'' and Z''). The geometric capacitance C_0 is used to calculate the dielectric constant k and the conductivity σ of the sample. For a thin disk of area A and thickness t, the geometric capacitance is obtained as $C_0 = \epsilon_0 A/t$, where ϵ_0 is the permittivity of free space. The dielectric constant is then $k = \epsilon'/C_0$, and the conductivity is $\sigma = \epsilon_0/(C_0 Z')$.

When modeled as a single resistance in parallel with a capacitance, the impedance takes the form of a semicircle.[29] If the measurements are taken down to a sufficiently low frequency, then the direct current (DC) resistance can be estimated from the intercept of the semicircle with the real axis. The DC conductivity can be written as:

$$\sigma_{DC} = \lim_{\omega \to 0} \epsilon_0/(C_0 Z') \qquad (2)$$

This method is preferred when the impedance is sufficiently high that it cannot easily be measured with DC methods.

The use of impedance spectroscopy in coordination polymers has been limited to thin films of metal-substituted organic complexes[30,31] and polymers with incorporated organometallic fragments.[31] Reports of the use of impedance spectroscopy to characterize pressed bulk powders of coordination polymers are virtually nonexistent in the literature. Crayston et al. published a study concerning the pressed powder conductivity of poly-$[RuCl_2(pdi)_{3/2}(\text{dimethyl sulfoxide})_1]$, a compound very similar to poly-[Rh(pdi)$^{+}_{4/2}$(Cl)$^{-}$].[32] Using the four-probe method, they measured a conductivity of 2×10^{-12} S·cm^{-1} for the Ru-based polymer. Another study looked at the conductivity of thick films of poly-chelate poly-[M(4,4-bis[(*N*-butane salicylaldehyde-diamine diamine-5)azo]biphenyl)], where M = Mn(II), Fe(II), Ni(II), Zn(II), Cd(II), measuring conductivities with an electrometer between 10^{-8} and 10^{-11} S·cm^{-1}.[33] An earlier report focused on the effect of moisture in poly-[Rh(pdi)$^{+}_{4/2}$(Cl)$^{-}$]. Using this technique, we were able to show a tendency for poly-[Rh(pdi)$^{+}_{4/2}$(Cl)$^{-}$] to become more conducting in a dry environment.[34]

The goal of this paper is to study the effect of structure and chemical stability on the electrical properties of coordination polymers. To our knowledge, this is the first full report to apply impedance spectroscopy over a large frequency range to insoluble coordination polymers. These measurements allow us to extrapolate DC conductivity of poly-[Rh(pdi)$^{+}_{4/2}$(Cl)$^{-}$] as well as the AC dielectric properties. This work also attempts to characterize the chemical stability of poly-[Rh(pdi)$^{+}_{4/2}$(Cl)$^{-}$] upon exposure to air using X-ray diffractometry (XRD), thermogravimetric analysis (TGA), and X-ray photoelectron spectroscopy (XPS).

2. Experimental Section

The chlorodicarbonylrhodium(I) dimer (Strem) and reagent grade CH_2Cl (Sigma-Aldrich, 99.5%) were used without purification. Pdi (Aldrich, 99%) was sublimed in vacuum to obtain white crystals. The polymerization was carried out at room temperature in a three-necked, round-bottom flask under nitrogen. 155 mg of $[Rh(CO)_2Cl]_2$ was dissolved in 26 mL of CH_2Cl_2 (used without distillation) and poured into the flask. 202 mg of pdi, a 2-fold molar excess, was dissolved in 50 mL of the same solvent and added dropwise to the $[Rh(CO)_2Cl]_2$. After 45 min, a dark green precipitate was obtained which was then filtered, washed with CH_2Cl_2 (4 × 50 mL), and dried overnight under vacuum at 5 in. of Hg at 110 °C.

The resulting powder was ball-milled for 7 h, pressed into pellets under uniaxial pressure of 5 tons for 20 min, and sputter-coated with platinum. The thickness of the pellets was measured by a micrometer, and the area was measured by analysis of digital photographs. This was necessary because the pellets were extremely brittle and had uneven shapes. Samples were placed in a specially designed test fixture and lowered into a Schlenk bottle for testing. Because of the porous nature of the solid, poly-[Rh(pdi)$^{+}_{4/2}$(Cl)$^{-}$] has been shown to adsorb up to half its own weight in ambient moisture, so control of environment was essential to creating reproducible data.[19] To control the temperature and humidity, the Schlenk bottle contained a small amount of desiccant at the bottom and was wrapped with flexible electric heating tape. The temperature inside the Schlenk tube was controlled by an Omega CN9122A PID controller, temperature readings were taken from a thermocouple inside the flask. Samples were stored under lab air at 21 °C from the time of synthesis until being tested. At the time of measurement, all samples had been heated to 100 °C under a vacuum of ∼5 in. of Hg.

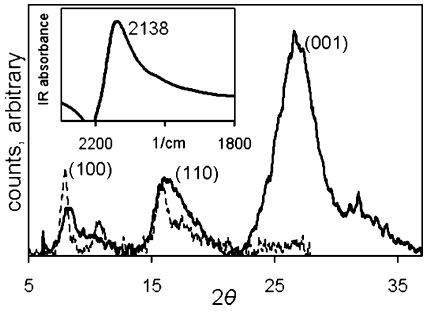

Figure 2. X-ray diffraction patterns (XRD) of poly-$[Rh(pdi)^{+}_{4/2}(Cl)^{-}]$. The peaks generated by the (1 0 0) and (1 1 0) planes (the $X-Y$ plane of the square-planar geometry) correspond to the length of the pdi ligand, and the peak from the (0 0 1) plane corresponds to the Rh−Rh stacking bond distance of 3.3 Å. The dashed line shows an X-ray diffraction pattern for unwashed poly-$[Rh(pdi)^{+}_{4/2}(Cl)^{-}]$, with no peak from the (0 0 1) plane present. The inset shows the ν(CN) absorbance peak of the poly-$[Rh(pdi)^{+}_{4/2}(Cl)^{-}]$ taken after drying.

Electrical experiments were conducted using a Solartron SI 1260 impedance analyzer and a 1296 Dielectric Interface in the frequency range of 10 mHz to 10 MHz with 0.1 V rms. Multiple impedance spectra were collected at each temperature to ensure representative behavior. Complex impedance plots were used to estimate the DC conductivity (with geometric considerations).

FT-IR spectra were collected from NaCl pellets by a Nicolet Nexus 870 Infrared spectrometer over 500 scans with 2 cm^{-1} resolution. X-ray diffraction scans were taken with a Phillips PW 1800 X-ray diffractometer with Cu Kα radiation. The thermogravimetric analyses were carried out on a TA Instruments Q50 thermogravimetric analyzer from room temperature up to 500 °C at a heating rate of 5 °C/min under nitrogen and oxygen. X-ray photoelectron spectroscopy was conducted on a Surface Science Instruments SSX-100 small spot ESCA spectrometer with Al Kα General Survey. The pass energy was 150 eV with a takeoff angle of 55° from the normal. All samples were charge compensated by indexing the aromatic C(1s) line at 284.8 eV.

3. Results and Discussion

3.1. Chemical Characterization of Poly-$[Rh(pdi)^{+}_{4/2}(Cl)^{-}]$. Tetragonal poly-$[Rh(pdi)^{+}_{4/2})(Cl)^{-}]$ was prepared from the reaction of chlorodicarbonylrhodium(I) dimer with two-fold molar excess of pdi under mild experimental conditions.[21] This reaction is shown as follows:

$$\left(\frac{n}{2}\right)[Rh(CO)_2Cl]_2 + 2n(pdi) \rightarrow [Rh(pdi)^{+}_{4/2}Cl^{-}]_n + 2n(CO) \quad (3)$$

Figure 2 shows the X-ray powder diffraction patterns as well as the FT-IR peak used to confirm the presence of poly-$[Rh(pdi)^{+}_{4/2}(Cl)^{-}]$. The IR peak shown corresponds well to the isocyanide stretching frequency, ν(CN), of 2140 cm^{-1} previously reported for poly-$[Rh(pdi)^{+}_{4/2}(Cl)^{-}]$.[35]

The X-ray trace shows the peak of the (1 0 0) plane at $2\theta = 7.7°$, corresponding to a spacing of 11.5 Å, the approximate length of a single pdi ligand molecule. The peak at $2\theta = 26°$ is assigned to the (0 0 1) plane and attributed to the close proximity of 3.3 Å between Rh(I) ions in adjacent, parallel ligand sheets.[19] Taking both peaks together, the X-ray diffraction pattern indicates that the polymer exists as layered graphite-like lamella, with interplanar spacings of 3.3 Å. Figure 2 also shows that thorough washing was found to play an important role in allowing the X-ray peaks of the (0 0 1) planes to be detected.

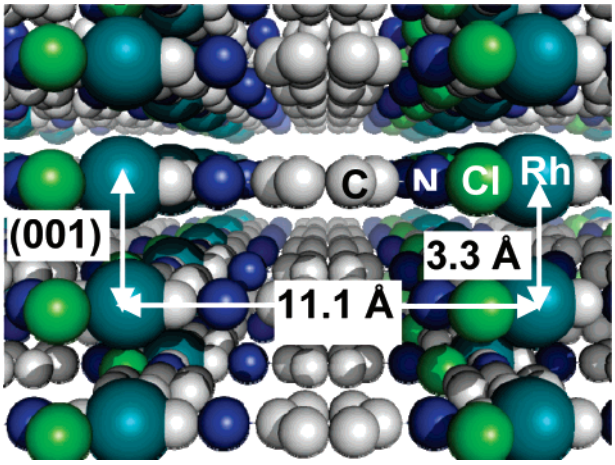

Figure 3. Representation of poly-$[Rh(pdi)^{+}_{4/2}(Cl)^{-}]$ as viewed perpendicular to the [0 0 1] direction. The H atoms are omitted for clarity. The close proximity of the Rh atoms creates a conducting pathway in the [0 0 1] direction.

On the basis of matching chemical and structural data, we conclude that the synthesized structure is similar to the one depicted schematically in Figure 3.

3.2. Electrical Characterization of Poly-$[Rh(pdi)^{+}_{4/2}(Cl)^{-}]$. Electrical measurements were conducted to determine the electrical activation energy for conduction and possible contribution of Rh−Rh bonds to the conductivity. By treating poly-$[Rh(pdi)^{+}_{4/2}(Cl)^{-}]$ as a semiconductor in the intrinsic region, the activation energy can be calculated according to eq 4:

$$\sigma(T) = \sigma_0 \exp\left(\frac{-E}{2kT}\right) \quad (4)$$

where E is the activation energy, T is the temperature in Kelvin, k is the Boltzmann constant, and σ_0 is the pre-exponential constant. As shown in Figure 4a,b, the real and imaginary conductivity exhibit frequency dispersion; so, it is important that the steady-state conductivity be reported and not the conductivity at a certain frequency. In keeping with eq 2, the DC conductivities are estimated by taking the reciprocals of the low frequency intercepts of the complex impedance curves, shown in Figure 4c (with geometry accounted for) or from the frequency independent flat region in Figure 4a. Our calculation of the electrical activation energy comes from the slope of the ln σ versus $1/T$ curves shown in the inset of Figure 4c. These curves indicate that the electrical activation energy of poly-$[Rh(pdi)^{+}_{4/2}(Cl)^{-}]$ is 0.9 eV.

Over time, the powder began to change color, going from a deep green to a dark brown. As the conductivities of more specimens were tested, it became apparent that the measured conductivity decreased as the specimens aged. After 36 days, the estimated σ_{DC} was less than 1% of its estimated initial value.

In order to examine the effect of the decrease in the bulk conductivity, the conductivities of the specimens collected at 45 °C were graphed as a function of time (i.e., measurement time after synthesis). This graph, displayed in Figure 5 along with the corresponding normalized impedance spectra, shows the conductivity to exhibit exponential decay with time t from synthesis, $\sigma(t) = \sigma(0)\exp(-t/\tau)$, with $\tau = 8$ days and $\sigma(0) = 1.4 \times 10^{-10} \pm 0.5$ S·cm^{-1} at 45 °C. By using the electrical activation energy, the room temperature $\sigma(0)$ can be estimated to be 3.4×10^{-11} S·cm^{-1}. This conductivity is much lower than the value of 4.4×10^{-4} S·cm^{-1} previously reported at 1 kHz for this material.[16] However, it is much closer to the

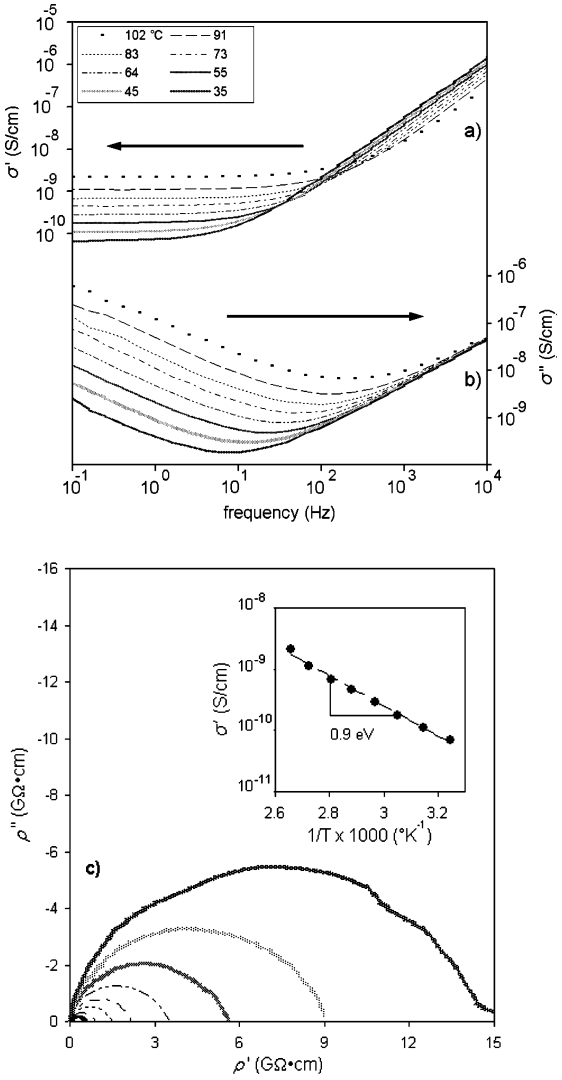

Figure 4. Real (a) and imaginary (b) conductivities of poly-$[Rh(pdi)^{+}_{4/2}(Cl)^{-}]$, respectively, show that they are frequency dependent. The complex resistivity curves of poly-$[Rh(pdi)^{+}_{4/2}(Cl)^{-}]$ for a range of temperatures from 101−35 °C are shown in c. The low frequency intercepts on the real axis indicate the estimated DC resistivity, from which the DC conductivity is calculated. The inset of c shows the conductivity plotted against $1/T$, indicating the electrical activation energy.

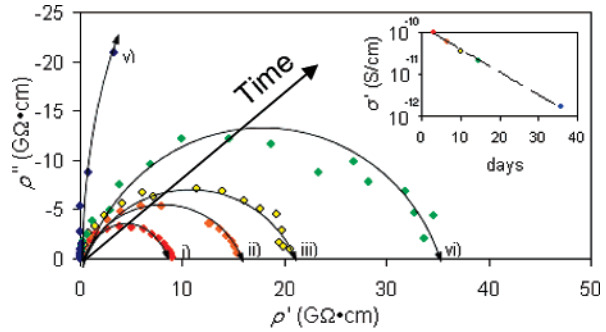

Figure 5. In (a), the complex impedance plots of poly-$[Rh(pdi)^{+}_{4/2}(Cl)^{-}]$ for 3, 7, 10, 14, and 36 days after synthesis are shown in i, ii, iii, iv, and v, respectively. All measurements were taken at 45 °C in an evacuated Schlenk tube. The inset shows the conductivities calculated from the low frequency intercepts of these curves, indicating that the material becomes less conductive with time. The dashed line indicates an exponential fit with a time constant of 8 days. conductivity of 2×10^{-12} S•cm^{-1} reported by Crayston et al.[32,36] for the poly-$[RuCl_2(pdi)_{3/2}(dmso)_1]$ complex.

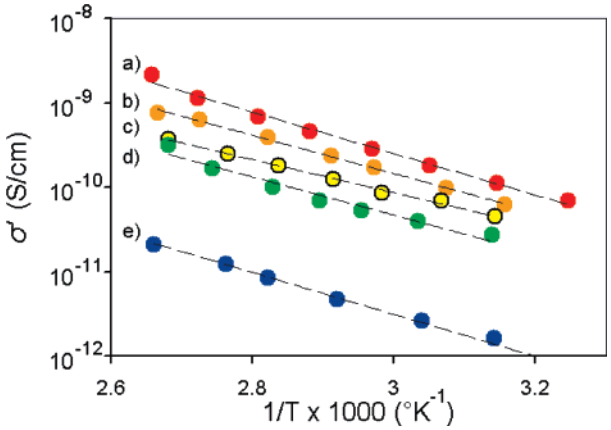

Figure 6. Frequency dependent dielectric constant at 10 kHz of poly-$[Rh(pdi)^{+}_{4/2}(Cl)^{-}]$ at 45 °C. The dielectric constant is shown to decrease over 36 days. The inset shows the temperature dependence of the dielectric constant at 10 kHz taken 3 days after synthesis.

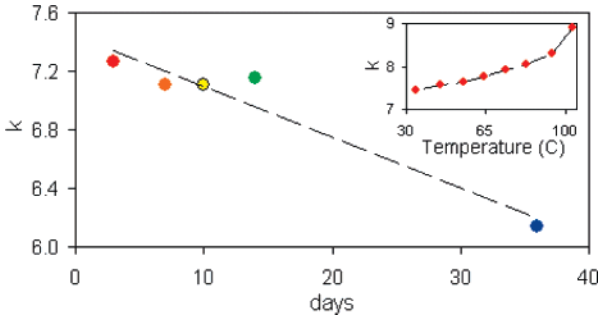

Figure 7. Plots indicating the electrical activation energy of poly-$[Rh(pdi)^{+}_{4/2}(Cl)^{-}]$ for 3, 7, 10, 14, and 36 days after synthesis are shown in a, b, c, d, and e, respectively. While the fitted activation energy remains relatively constant at 0.9 eV, the magnitude of the conductivity drops with increasing time in air.

The time-dependent behavior displayed in Figure 5 was not temperature specific but occurred throughout the range of temperatures measured. Figure 6 shows the activation energy plots for specimens from 3 to 36 days after synthesis. Despite the decrease in the conductivity, the activation energy remains consistent around 0.9 eV. This would appear to indicate that the basic conduction mechanism remains the same, since a change in the electrical activation energy would be evidence of a different mechanism.

While not as drastic, the dielectric constant of poly-$[Rh(pdi)^{+}_{4/2}(Cl)^{-}]$ was also found to decrease as a function of time with exposure to air. To our knowledge, the dielectric properties of these polymers have never been reported. Figure 7 shows the dielectric constant with an estimated initial value of 7.5 at room temperature and decreasing by 15% over 36 days. Data are reported at a frequency of 10 kHz because the dielectric constant is independent of frequency in this range while it is sensitive to dispersion at lower frequencies. A sample of commercial copper phthalocyanine (CuPc) was used to verify the accuracy of our apparatus. Our measurement of the dielectric constant of pressed pellets of CuPc was 3.9 at 10 kHz. This compared favorably with the DC dielectric constant reported for CuPc thin-films of 3.6, with the difference being attributed to a small amount of space charge-limited current at the grain boundaries of the pressed powder sample.[37]

The process of pressing the bulk powder leaves a fraction of the volume of the pellet occupied by porosity. This lowers the density of the pellet and consequently also the measured dielectric constant. While we were not able to determine the

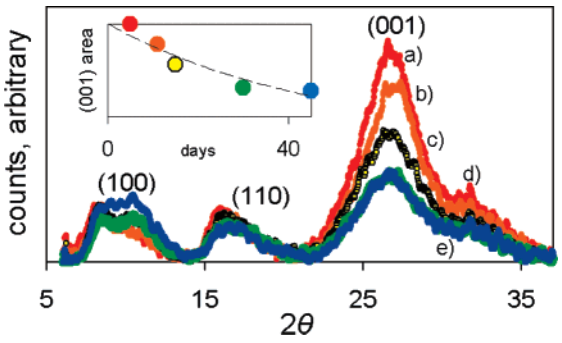

Figure 8. X-ray diffraction scans of poly-[Rh(pdi)$^{+}_{4/2}$(Cl)$^{-}$] for 5, 11, 15, 31, and 45 days are shown in a, b, c, d, and e, respectively. The change of the (0 0 1) peak height with days from synthesis is shown in the inset. Note that the peaks from the (1 0 0) and (1 1 0) planes do not change appreciably over time.

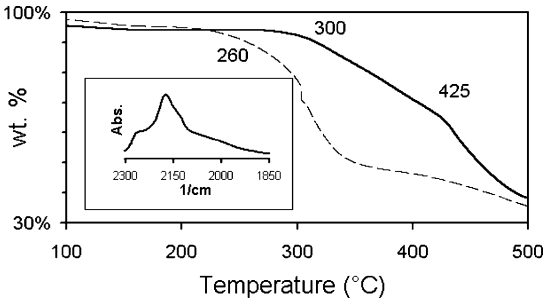

Figure 9. TGA of poly-[Rh(pdi)$^{+}_{4/2}$(Cl)$^{-}$] under both nitrogen (line) and oxygen (dashed line). Note the existence of two decomposition temperatures, at 300 and 425 °C under N_2. Under air, the decomposition starts at 260 °C. This coincides with the boiling point of 1,4-diisocyanatobenzene. The FTIR of poly-[Rh(pdi)$^{+}_{4/2}$(Cl)$^{-}$] after being heated to 260 °C under oxygen is shown in the inset. The shoulder at 2267 cm^{-1} is indicative of the ν(CN) of an isocyanate.

volume fraction of the porosity in the specimens, the dielectric constant of the pure polymer with no porosity is likely to be higher. In terms of the dielectric constant, the polymer can be modeled as a collection of one-dimensionally conducting regions where the charge carriers (electrons) have very high mobility.[38] Lattice translations or crystal defects could effectively reduce the length of these regions and reduce the polarizability and the dielectric constant.

3.3. Structural Characterization of Poly-[Rh(pdi)$^{+}_{4/2}$(Cl)$^{-}$]. The long-range Rh−Rh stacking columns are the most structurally important features of this polymer. As these have been shown to be the most electrically conductive bonds in the material,[17] the existence of the peak in the X-ray diffraction pattern corresponding to the (0 0 1) plane is of primary importance if a one-dimensional metal is desired. Figure 8 shows a series of X-ray scans of poly-[Rh(pdi)$^{+}_{4/2}$(Cl)$^{-}$] over a period of 45 days. The specimens were left exposed to open atmosphere from the time of synthesis until analysis. These scans show the evolution of the crystal structure in the polymer over that time. Although the peak heights of the (1 0 0) and the (1 1 0) planes remain constant, the peak of the (0 0 1) plane decreases in intensity over the course of a month to half its original value. Because the samples were stored in air, an oxidative process is suspected of introducing disorder into the delicate lattice supporting the extended Rh−Rh chains. This would indicate a reduction in Rh−Rh interactions over time, possibly due to chemical attack at the isocyanide moiety.

The likely culprit for such a degradation mechanism is the isocyanide−metal bond. The long-term oxidative stability of isocyanide−metal junctions has been the subject of recent research.[4,38−42] Impurities have been shown to arise in different isocyanides for self-assembled monolayers on gold,[4,39,40] nickel,[41] and copper,[42] as well as cobalt-diisocyanobenzene multilayer thin films.[43] Although no such degradation studies have been carried out on Rh surfaces, diisocyanides have been shown to bond to Rh linearly through a single isocyanide group, similar to the bonding on Au (1 1 1).[44−46] Rhodium has also been shown to catalyze polyisocyanides, possibly making the isocyanide sensitive to attack from oxygen or atmospheric ozone.[4,47−50] This would imply that there are at least two routes to oxidative degradation available to poly[Rh(pdi)$^{+}_{4/2}$(Cl)$^{-}$]: conversion from isocyanide to isocyanate and polymerization to form polyisocyanides.

Although a molecular wire on a smooth metal surface depends on a one-dimensional bonding mechanism for conduction, poly-[Rh(pdi)$^{+}_{4/2}$(Cl)$^{-}$] has bonding in two dimensions, in-plane and out-of-plane. This means that the conductivity is extremely sensitive to even a small change in the concentration of the connected Rh−Rh molecular wires. This sensitivity is evident in these experiments, where a reduction in the Rh−Rh bonded regions by a factor of 2 has caused the conductivity to decrease by a factor of 100. This might also explain the decrease in the dielectric constant. The drop in dielectric constant is explained in terms of a decrease in the average length of the domain that a charge carrier can traverse. Initially, the material has a large polarizability because of the mobility of charge carriers on these extended conductive regions. The length of these highly conductive domains decreases as the metal−metal bonding decreases. This would cause the polarizability to decrease, decreasing the dielectric constant. In light of these results, a degradation mechanism, similar to that observed in SAMs,[4] is proposed to cause the change in the electrical properties of poly-[Rh(pdi)$^{+}_{4/2}$(Cl)$^{-}$].

3.4. Thermal Degradation of Poly[Rh(pdi)$^{+}_{4/2}$(Cl)$^{-}$]$_n$. Thermogravimetric analysis (TGA) is one way to probe the strength of these bonds and their chemical sensitivity. However, we also wanted to investigate the effect of atmosphere on thermal degradation. Figure 9 shows a comparison between two TGA curves taken under oxygen and nitrogen. Under nitrogen, we observed an initial decomposition at 300 °C and a secondary one at 425 °C, consistent with a previous report.[21] Under oxygen, the initial decomposition starts at 260 °C and is accompanied by the appearance of an absorbance peak at 2270 cm^{-1} in the FT-IR spectrum, visible in the inset of Figure 9. This absorbance peak in the IR would indicate an isocyanate (N═C═O) is most likely present in the polymer.[4] Because the boiling temperature of 1,4-phenylene diisocyanate is 260 °C, the conversion of diisocyanide to diisocyanate would proceed according to the reaction below:

$$(\mathrm{Rh{-}CN{-}\Phi{-}NC{-}Rh})_2\mathrm{Cl}_{(s)}^{-} \xrightarrow[260^\circ]{\mathrm{O_2}} 2\mathrm{RhCl}_{(s)} + 2(\mathrm{OCN{-}\Phi{-}NCO})_{(g)} \quad (5)$$

This process is certainly accelerated in the TGA by high temperature and the presence of an oxygen-rich environment, but it may occur more slowly in air at room temperature. In addition, the close proximity of adjacent Rh(I) atoms might enable them to insert O^{-2} into nearby isocyanide moieties through diatomic cleavage.[51] If so, it would indicate that the degradation process involves the insertion of oxygen into the N≡C−Rh bond to form a N═C═O(Rh) complex. The effect of this oxidation would be not only to stop any in-plane conduction, but also to disrupt Rh−Rh bonding, decreasing the crystallinity of the material and lowering the conductivity.

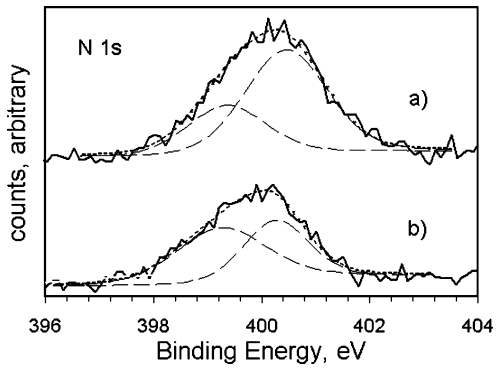

Figure 10. High-resolution XPS of the N(1s) region of poly-$[Rh(pdi)^{+}_{4/2}(Cl)^{-}]$. In (a), a pressed pellet has been stored under Ar, with little exposure to air for one week. In (b), another pressed pellet has been stored under lab air for the same amount of time.

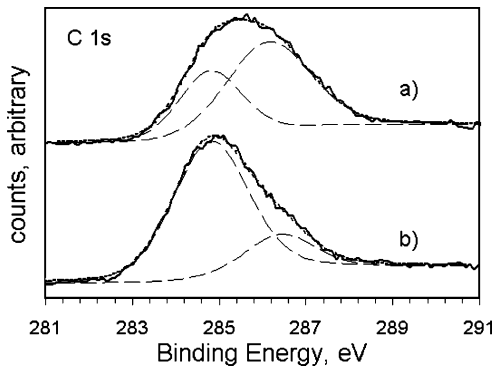

Figure 11. High-resolution XPS of the C(1s) region of poly$[Rh(pdi)^{+}_{4/2}(Cl)^{-}]$. In (a), a pressed pellet has been stored under Ar, with little exposure to air for one week. In (b), another pressed pellet has been stored under lab air for the same amount of time.

3.5. X-ray Photoelectron Spectroscopy of Poly $[Rh(pdi)^{+}_{4/2}(Cl)^{-}]$. XPS has been used to characterize the presence of non-isocyanide chemical species present in the metal−isocyanide systems. Accordingly, XPS measurements were performed to probe whether there were any shifts in the binding energies of the N(1s) and C(1s) electrons that would indicate a particular degradation process. By analysis of chemical shifts in the N(1s) binding energy, the presence of a non-isocyanide species in poly$[Rh(pdi)^{+}_{4/2}(Cl)^{-}]$ would be apparent. A binding energy between 399.9−400.6 eV has been assigned to metal bonded isocyanides.[41,43] N(1s) peaks with lower binding energies in these systems, from 399.3 to 398.7, have been assigned to polyisocyanides[4,41,43] and isocyanates.[4]

To differentiate between any non-oxidative degradation and oxidative degradation, two samples of poly$[Rh(pdi)^{+}_{4/2}(Cl)^{-}]$ were held under different atmospheres for one week. Sample A was held under argon, and sample B was held under lab air. High-resolution XPS scans of the N(1s) peak of both samples are shown in Figure 10. The sample held under Ar showed two peaks when deconvoluted: a smaller peak centered at 399.3 eV and a larger one 400.6 eV. Upon extended exposure to lab air, the resulting spectrum shows the peak at 400.1 eV greatly reduced but the peak centered at 399.3 eV now much larger, consistent with a conversion from isocyanide to isocyanate. In like manner, the C(1s) peak, shown in Figure 11, can be fitted with two curves. In both samples, the lower binding energy (BE) peak at 284.8 is fitted to aromatic carbon. Because of the strong upward shift observed in the C(1s) peak observed for isocyanides,[52] the higher BE peak, at 286.2 for the sample stored in argon and 286.4 in air, is assigned to carbon in isocyanide. The isocyanide peak is the larger of the two in the sample stored under argon but is the smaller of the two in the sample stored under air. This shift to a lower binding energy could be attributed to adventitious carbon, but that is unlikely, as both samples were stored in sealed containers under identical conditions (except for atmosphere). Instead, the decrease is attributed to the conversion of isocyanide to a lower BE isocyanate, similar to the decrease in BE observed in methyl isocyanide.[52]

It can be speculated that the effect of the high-temperature oxidation is the same as that observed in the room-temperature oxidation of poly$[Rh(pdi)^{+}_{4/2}(Cl)^{-}]$. Evidence for this is given by the decrease in the metal−isocyanide bonding present in the polymer and the disruption of the metal−ligand lattice necessary for metallic conduction. It should be noted that the lower BE peak could also be caused by a conversion of isocyanide to polyisocyanide, generally denoted by an N(1s) peak in the XPS around 398.7.[4,7,41,43] While we cannot rule this out, we do not expect it because the IR showed no evidence for the formation of polyisocyanides in the polyimide region (1570−1670 cm^{-1}).

There are some IR peaks that do not support the proposed oxidation mechanism from poly$[Rh(pdi)^{+}_{4/2}(Cl)^{-}]$ to poly[RhCl(phenylene diisocyanate)]. Although a shoulder at 2267 cm^{-1} was visible after high-temperature oxidation, this feature did not appear in room-temperature samples, even after long aging times. Moreover, there was no noticeable decrease in the isocyanide peak at 2138 cm^{-1}. It is possible that, at room temperature, the oxidation occurs principally at the surface of the specimen pellets, while the interior remains largely unaffected. This would imply that a pellet of this powder would be composed of crystalline, conductive grains surrounded by an oxidized shell of amorphous insulating materials. The O(1s) peak in the XPS was also found to be invariant upon exposure to atmosphere, appearing in samples stored both in air and in Ar. If a conversion from N≡C−Rh → N=C=O(Rh) were indeed taking place, then the O(1s) signal in the XPS would have been expected to increase accordingly. However, the presence of the O(1s) peak may also be attributed to some unreacted carbonyl in the specimens or contamination by ambient moisture prior to insertion into the XPS chamber.[19] Even so, our data indicate that the changes in conductivity, dielectric constant, color, and crystallinity are not coincidental but directly caused by an oxidative process occurring in ambient conditions.

4. Conclusions

The estimated electrical conductivity of poly$[Rh(pdi)^{+}_{4/2}(Cl)^{-}]$ of 3.4×10^{-11} S·cm^{-1} at room temperature is far less than what had originally been reported.[16] The present research indicates that this conductivity showed a strong dependence on the metal−metal stacking interactions of the Rh atoms in the polymer. The drop in the intensity of the peak of the (0 0 1) plane, attributed to a loss in Rh−Rh bonding and the conductivity upon exposure to air show a direct correlation with one another. This sensitivity to air is attributed to the oxidation of the ligands coordinated to the Rh atoms. Thermogravimetric analysis measured in oxygen indicates that there is a decomposition that takes place at 260 °C, which is attributed to an isocyanide−isocyanate conversion. Evidence of this conversion is also seen in the N(1s) and C(1s) regions of the XPS, where exposure to air appears to produce an isocyanate group in the polymer. This research shows that further attention is required before poly$[Rh(pdi)^{+}_{4/2}(Cl)^{-}]$ and, for that matter, any other materials that incorporate metal−isocyanide bonds see widespread use as conductors. Despite these difficulties, this study provides a better understanding of the dielectric properties

that these coordination polymers exhibited and a promising basis for promoting their potential utilization as soft, organic dielectric materials.

Acknowledgment. The authors thank the Institute for Paper Science and Engineering at the Georgia Institute of Technology for their generous support of this research, as well as Dr. Brent Carter for providing use of the X-ray photoelectron spectroscopy equipment. Rosario A. Gerhardt acknowledges funding from The National Science Foundation under Award No. DMR-0633456. Rina Tannenbaum acknowledges funding from The National Science Foundation, under Award No. ECS-0535382. Rina Tannenbaum is also with the department of Chemical Engineering, Technion, Israel, where she is supported by a Marie Curie Grant through the European Union (EU) and by the Israel Science Foundation, Grant 650/06.

References and Notes

(1) Hong, S.; Reifenberger, R.; Tian, W.; Datta, S.; Henderson, J. I.; Kubiak, C. P. *Superlattices Microstruct.* **2000**, *28*, 289.
(2) James, D. K.; Tour, J. M. *Chem. Mater.* **2004**, *16*, 4423.
(3) Lang, N. D.; Avouris, P. *Phys. Rev. B* **2001**, *6412*.
(4) Stapleton, J. J.; Daniel, T. A.; Uppili, S.; Cabarcos, O. M.; Naciri, J.; Shashidhar, R.; Allara, D. L. *Langmuir* **2005**, *21*, 11061.
(5) Martin, A. S.; Sambles, J. R.; Ashwell, G. J. *Phys. Rev. Lett.* **1993**, *70*, 218.
(6) Metzger, R. M. *Chem. Rev.* **2003**, *103*, 3803.
(7) Lee, J. O.; Lientschnig, G.; Wiertz, F.; Struijk, M.; Janssen, R. A. J.; Egberink, R.; Reinhoudt, D. N.; Hadley, P.; Dekker, C. *Nano Lett.* **2003**, *3*, 113.
(8) Chen, J.; Reed, M. A.; Rawlett, A. M.; Tour, J. M. *Science* **1999**, *286*, 1550.
(9) Carroll, R. L.; Gorman, C. B. *Angew. Chem., Int. Ed.* **2002**, *41*, 4379.
(10) Dupraz, C. J. F.; Beierlein, U.; Kotthaus, J. P. *Chem. Phys. Chem.* **2003**, *4*, 1247.
(11) Batten, S. R.; Murray, K. S. *Coord. Chem. Rev.* **2003**, *246*, 103.
(12) Dinolfo, P. H.; Williams, M. E.; Stern, C. L.; Hupp, J. T. *J. Am. Chem. Soc.* **2004**, *126*, 12989.
(13) Hirao, T. *Coord. Chem. Rev.* **2002**, *226*, 81.
(14) Kingsborough, R. P.; Swager, T. M. Transition metals in polymeric pi-conjugated organic frameworks. *Prog. Inorg. Chem.* **1999**, *48*, 123.
(15) Petitjean, A.; Puntoriero, F.; Campagna, S.; Juris, A.; Lehn, J. M. *Eur. J. Inorg. Chem.* **2006**, 3878.
(16) Feinstein-Jaffe, I.; Efraty, A. *Macromolecules* **1986**, *19*, 2076.
(17) Lawrence, S. A.; Lott, K. A. K.; Sermon, P. A.; Short, E. L.; Feinstein-Jaffe, I. *Polyhedron* **1987**, *6*, 2027.
(18) Efraty, A.; Feinstein, I. *Inorg. Chem.* **1982**, *21*, 3115.
(19) Efraty, A.; Feinstein, I.; Frolow, F.; Wackerle, L. *J. Am. Chem. Soc.* **1980**, *102*, 6341.
(20) Efraty, A.; Feinstein, I.; Wackerle, L.; Frolow, F. *Angew. Chem., Int. Ed. Engl.* **1980**, *19*, 633.
(21) Feinstein-Jaffe, I.; Frolow, F.; Wackerle, L.; Goldman, A.; Efraty, A. *J. Chem. Soc., Dalton Trans.* **1988**, 469.
(22) Lawrence, S. A.; Sermon, P. A.; Feinstein-Jaffe, I. *J. Mol. Catal.* **1989**, *51*, 117.
(23) Tannenbaum, R. *Chem. Mater.* **1994**, *6*, 550.
(24) Tannenbaum, R. *J. Mol. Catal.* **1996**, *107*, 207.
(25) Tannenbaum, R. *Inorg. Chim. Acta* **1988**, *148*, 199.
(26) Jonscher, A. K. *Dielectric Relaxation in Solids*; Chelsea Dielectrics Press: London, U.K., 1983.
(27) Cao, W. Q.; Gerhardt, R. *Solid State Ionics* **1990**, *42*, 213.
(28) Gerhardt, R. A. Impedance Spectroscopy and Mobility Spectra. In *Encyclopedia of Condensed Matter Physics*; Bassani, G., Leidl, G., Wyder, P., Eds.; Elsevier: Boston, 2005; p 350.
(29) Gerhardt, R. *J. Phys. Chem. Solids* **1994**, *55*, 1491.
(30) Dakhel, A. A.; Ali-Mohamed Ahmed, Y. *J. Phys. Chem. Solids* **2005**, *66*, 1080.
(31) Diaz, C.; Valenzuela, M. L.; Barbosa, M. *Mater. Res. Bull.* **2004**, *39*, 9.
(32) Crayston, J. A.; Cupertino, D. C.; Forster, H. S. *Synth. Met.* **1990**, *35*, 365.
(33) Bansod, A.; Aswar, A. *Chin. J. Chem.* **2007**, *25*, 154.
(34) Carson, C. G.; Gerhardt, R. A.; Tannenbaum, R. *PMSE Prepr.* **2007**, *96*, 238.
(35) Jaffe, I. *Rev. Inorg. Chem.* **1993**, *13*, 1.
(36) Crayston, J. A.; Cupertino, D. C.; Dines, T. J. *Dalton Trans.* **1991**, 1603.
(37) Gould, R. D. *Thin Solid Films* **1985**, *152*, 63.
(38) Pohl, H. A.; Pollak, M. *J. Phys. Chem.* **1977**, *66*, 4031.
(39) Huc, V.; Bourgoin, J. P.; Bureau, C.; Valin, F.; Zalczer, G.; Palacin, S. *J. Phys. Chem. B* **1999**, *103*, 10489.
(40) Lin, S.; McCarley, R. L. *Langmuir* **1999**, *15*, 151.
(41) Pranger, L.; Tannenbaum, R. *J. Colloid Interface Sci.* **2005**, *292*, 71.
(42) Pranger, L.; Goldstein, A.; Tannenbaum, R. *Langmuir* **2005**, *21*, 5396.
(43) Ansell, M. A.; Cogan, E. B.; Page, C. J. *Langmuir* **2000**, *16*, 1172.
(44) Gruenbaum, S. M.; Henney, M. H.; Kumar, S.; Zou, S. Z. *J. Phys. Chem. B* **2006**, *110*, 4782.
(45) Robertson, M. J.; Angelici, R. J. *Langmuir* **1994**, *10*, 1488.
(46) Semancik, S.; Haller, G. L.; Yates, J. T. *J. Chem. Phys.* **1983**, *78*, 6970.
(47) Onitsuka, K.; Mori, T.; Yamamoto, M.; Takei, F.; Takahashi, S. *Macromolecules* **2006**, *39*, 7224.
(48) Onitsuka, K.; Yamamoto, M.; Mori, T.; Takei, F.; Takahashi, S. *Organometallics* **2006**, *25*, 1270.
(49) Tabei, J.; Shiotsuki, M.; Sanda, F.; Masuda, T. *Macromolecules* **2005**, *38*, 9448.
(50) Arshady, R.; Zecca, M.; Corain, B. *React. Polym.* **1993**, *20*, 147.
(51) Rasko, J.; Kiss, J. *Appl. Catal., A* **2006**, *298*, 115.
(52) Clark, D. T.; A. H. *J. Polym. Sci. Polym. Chem.* **1981**, *19*, 1945.